Letters

On the Transient Overcurrent Mechanism of Grid Forming Converter in Fault Recovery Stage

Boxin Liu, *Graduate Student Member, IEEE*, Xin Xiang, *Member, IEEE*, Yonghao Li, *Student Member, IEEE*, Yi Long, Tianling Shi, *Member, IEEE*, Huan Yang, *Member, IEEE*, Wuhua Li, *Senior Member, IEEE*, and Xiangning He, *Fellow, IEEE*

***Abstract*—The grid forming (GFM) converter may undesirably output a higher current during the recovery stage than fault duration due to its transient angle swing, which would cause the power devices to face the risk of overcurrent or even damage in both the fault stage and the recovery stage. In this letter, the current power angle plane is presented for the current trajectory description and the mechanism of the recovery overcurrent (ROC) issue is revealed through the proposed concept of critical recovery angle (CRA). On top of that, the power angle relationship in the critical ROC state is described in detail and the ROC boundary is further characterized accurately. Moreover, an analytical calculation method of CRA is proposed to identify whether the ROC phenomenon occurs, which is well validated by a series of experiments. The proposed method depicts the inherent relationship between the current behavior and power angle motion of GFM converters quantitatively and intuitively, and it may provide some new insights into the transient analysis and control optimization of GFM converters.**

***Index Terms*—Critical recovery angle (CRA), current behavior, grid forming, recovery overcurrent (ROC) boundary, transient analysis.**

I. Introduction

With the significantly increasing penetration of power electronics-based resources in power systems, the grid forming (GFM) converter has attracted much attention because of its capability to establish the system voltage and frequency autonomously [1], [2]. The GFM control has been able to imitate or even surpass the static characteristics of a synchronous generator (SG), but its transient GFM properties under large disturbances have not been widely and deeply developed and studied due to the limited overcurrent capability (OCC) of power converters [3]. Although several advanced current limiters can reshape the port characteristics as a voltage source while limiting current [4], they still cannot provide sufficient fault support due to the lack of OCC and might lead to additional risks of large signal instability issues [5]. In recent research, the breakthroughs and innovations in device package, gate driver, modulation, and active thermal control enable power electronic converters to have short-term OCC [6], [7], [8], such as 3 p.u. current in 3 s [6], [7]. As a result, the converter starts to have the capability to maintain a transient voltage source behavior to autonomously support the voltage and frequency in the grid fault process with its GFM control [1], [9].

Because of the inherent power angle swing motion introduced by the synchronization mechanism, the GFM control will go through two stages during the grid fault process, namely the fault duration stage and post fault recovery stage [10]. Thanks to the development in transient analysis tools including equal area criterion [9], [17], Lyapunov-based method [11], and phase portrait method [12], the power angle motion in these two stages and its transient stability boundary can be accurately characterized. However, the power angle swing under stability constraints will further cause large signal variation in the current of the GFM converter. The converter would have to face the risk of transient overcurrent in both the fault stage [13] and the recovery stage [11]. The uncertainty of the overcurrent stage will result in additional constraints in the GFM converter due to its limited and costly OCC, unlike the conventional SG.

To quantitively describe the impact of current limitations on GFM converter operation, the current related constraints are transformed into the power angle range [14], but it only simply gives the maximum angle value in the angle curve and lacks the specific consideration of grid fault conditions. The fault impedance analysis method is proposed to present the impact of fault grid parameters and current characteristics simultaneously [15], but it only describes the static limitation of the fault current and does not discuss the current in the recovery stage. After modeling the post fault grid, the current curves in the fault stage and recovery stage can be characterized similarly [16], but the description of the transient transition process of current from the fault stage to the recovery stage is ignored, which results in the analysis of the overcurrent stage still missing. In summary, the state-of-the-art existing researches usually give a static

Manuscript received 30 March 2024; revised 30 April 2024 and 3 June 2024; accepted 13 June 2024. Date of publication 24 June 2024; date of current version 4 September 2024. This work was supported in part by the National Natural Science Foundation for Distinguished Young Scholars under Grant 51925702 and in part by the National Natural Science Foundation of China under Grant 52107214. *(Corresponding authors: Xin Xiang; Tianling Shi.)*

The authors are with the College of Electrical Engineering, Zhejiang University, Hangzhou 310027, China (e-mail: liuboxin@zju.edu.cn; xiangxin@zju.edu.cn; yhlee@zju.edu.cn; 22310078@zju.edu.cn; TL_Shi@163.com; yanghuan@zju.edu.cn; woohualee@zju.edu.cn; hxn@zju.edu.cn).

Color versions of one or more figures in this article are available at https://doi.org/10.1109/TPEL.2024.3418044.

Digital Object Identifier 10.1109/TPEL.2024.3418044

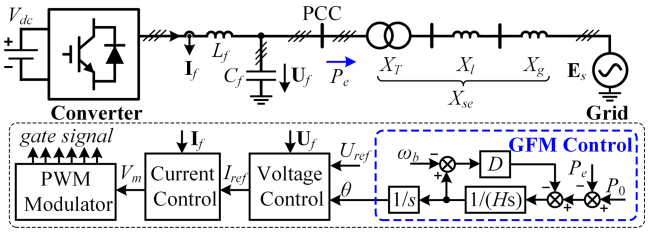

Fig. 1. Circuit and control structure of the grid-connected GFM converter.

description of the current behavior in fault and recovery stages with independent current characteristic curves, and the analysis of the transition trend from fault current to recovery current at the fault clear moment is still deficient. The unclear current transient characteristics make it very difficult to directly identify whether the maximum current occurs in the fault or recovery stage, which brings large challenges to the safe operation of GFM converters in the transient process.

This letter presents the current power angle plane for the current transient trajectory description of the grid-connected GFM converters, and it reveals the mechanism of the recovery overcurrent (ROC) with the concept of critical recovery angle (CRA). When the fault clear angle exceeds CRA, the GFM converter will output a larger current in the recovery stage for power angle deceleration and reactive power balance, which directly leads to the occurrence of the ROC phenomenon. On this basis, the power angle relationship in the critical ROC state is deduced with dual consideration of the transient current behavior in the fault and recovery process. Also, the ROC boundary is characterized in detail with the combination of the proposed angle relationship and the Lyapunov function. Moreover, the CRA is calculated analytically to readily evaluate whether the GFM converter has the ROC behavior. The major contributions of this letter are summarized as follows.

1) The mechanism of ROC is revealed through the presented current power angle plane.
2) The ROC boundary is characterized quantitively with a deduced power angle relationship in a critical ROC state.
3) The concept of CRA and its analytical calculation method is proposed. The ROC state can be readily and effectively identified by comparing the fault clear angle and CRA.

This letter depicts the inherent relationship between current behavior and angle swing motion quantitatively and intuitively, which may provide some new insights for the transient analysis and control optimization of the GFM converter.

II. System Description and Current Behavior Analysis

This section briefly presents the typical structure of the grid-connected GFM converter first and then investigates the current behavior through the proposed current power angle plane in detail.

A. System Modeling of GFM Converter

The typical control structure of the grid-connected GFM converter and its representative circuit are shown in Fig. 1. To depict the inherent and fundamental relationship between current behavior and power angle motion, the analysis and investigation of GFM converter with transient voltage source characteristics under good OCC is chosen as a starting point. With the rapid development of OCC enhancement technology in recent years, this solution would have good potential to provide urgent fault grid support while avoiding additional stability problems caused by current limiting control and nonlinear control mode switching. Also, the analysis can be extended to analyze more complex current behavior with additional control loops and physical design effects.

The GFM control is equipped as an outer power loop for grid synchronization. The constant terminal voltage (CTV) control is used, which can maintain the magnitude of terminal voltage U_f constant within the allowable range of current output capability and avoid overvoltage issues during grid fault transient [1], [2]. The CTV mode is also beneficial for the intuitive study of the inherent relationship between power angle swing and the transient current characteristics, since U_f will not change with the power angle motion and fault grid condition [9], [17]. Current $\mathbf{I}_f$ and voltage $\mathbf{U}_f$ are regulated by current/voltage dual-loop vector control, which consists of the current inner loop and voltage outer loop [1]. The dynamics of inner loops, which are generally over ten times larger than that of the power loop [1], [9], could be simplified due to the decoupled timescales. Thus, the terminal voltage U_f can achieve zero-error tracking of the voltage reference U_{ref} in the transient analysis, i.e., $\mathrm{U}_f = U_{\mathrm{ref}}$.

Since the symmetrical fault scenarios could usually reflect more essential characteristics of the GFM converter [12], the theoretical research is mainly derived and verified in the operating conditions of symmetrical grids, and it has the potential to be extended in asymmetric fault conditions by considering the large signal model of negative sequence. The transient behavior of grid-connected GFM converters in the fault process is dominated by its power angle dynamics and it can be described by the swing equation [9], [15], which is written as

$$H\ddot{\delta} = P_0 - P_e - D\dot{\delta} = P_0 - E_s U_f \sin\delta / X_{se} - D\dot{\delta} \quad (1)$$

where $\delta = \theta - \theta_s$ is defined as the power angle, and it is the phase difference between the terminal voltage $\mathbf{U}_f$ and grid voltage $\mathbf{E}_s$. X_{se} is the equivalent impedance between the point of common coupling and the grid. H and D are the inertia and damping coefficients in GFM control, respectively.

B. Current Behavior Analysis in Current Power Angle Plane

The apparent power $\mathbf{S}_{\mathrm{e}}(\delta)$ of the GFM converter is calculated with its terminal voltage vector $\mathbf{U}_f = U_f e^{-j0}$ and grid voltage vector $\mathbf{E}_s = E_s e^{-j\delta}$ as

$$\mathbf{S_e}(\delta) = P_e(\delta) + jQ_e(\delta) = U_f\left[\left(U_f - E_s e^{-j\delta}\right)/jX_{se}\right]^*. \quad (2)$$

The current under CTV control can be further derived as

$$I_e(\delta) = |\mathbf{S_e}(\delta)|/|\mathbf{U_f}| = \sqrt{P_{\mathrm{e}}(\delta)^2 + Q_{\mathrm{e}}(\delta)^2}\Big/U_f. \quad (3)$$

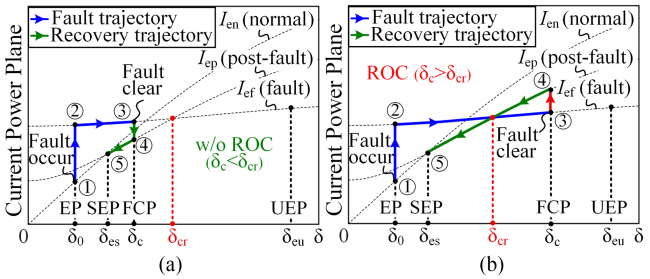

Fig. 2. Fault current trajectory in current power plane. (a) Fault recovery without ROC phenomenon (δ_c<δ_{cr}). (b) Fault recovery with ROC phenomenon (δ_c>δ_{cr}).

On substituting (2) into (3), the expression of transient current is

$$I_e(\delta) = \sqrt{E_s^2 + U_f^2 - 2U_f E_s \cos\delta} \Big/ X_{se}. \tag{4}$$

It can be seen that I_e will increase as the δ increases and X_{se} decreases. However, the relationship between I_e and E_s is not monotonic. At a small value of δ, the drop in E_s will lead to an increase in I_e, but it will lead to a decrease in current at a large δ. This means that after the fault is cleared at different δ values, the change of the current I_e may be completely opposite. Since current is the function of power angle, the current power angle plane with δ on the horizontal axis and I_e on the vertical axis can visually describe the current behavior in the fault and recovery stage, and the current will move along the $I_e(\delta)$ curve in this plane as the angle swing. The case where the grid voltage drops symmetrically to 0.1 p.u. and recovers to 0.9 p.u. with $X_{se} = 0.51$ p.u. is used for the discussion of transient current behavior. Due to the changes at grid voltage $\mathbf{E}_s$ of different fault stages, there are three $I_e(\delta)$ curves plotted from (4) as the black dotted lines in Fig. 2, and they show the large signal relationship between the power angle and the current at different stages. The inertia is temporarily ignored for intuitive analysis, and the steady-state current is $I_{en}(\delta_0)$ at the equilibrium point (EP) δ_0.

When the fault occurs, the current reaches $I_{ef}(\delta_0)$ and further increases slowly with the power angle until the fault clear point (FCP) δ_c. Taking the transient stability limitation into account, the range of power angle motion is from EP to unstable equilibrium point (UEP) [15]. Since there is an intersection point of fault current curve $I_{ef}(\delta)$ and post fault current curve $I_{ep}(\delta)$, there are two possible cases for the recovery current behavior determined by the angle at FCP. If the fault is cleared before the angle reaches δ_{cr}, the current in the recovery stage will be lower than that in the fault stage, as shown in Fig. 2(a). But if the angle exceeds δ_{cr} at FCP shown in Fig. 2(b), the ROC phenomenon will occur. Although the transient stability is guaranteed in the ROC state, the undesirable higher current in the recovery stage will cause the GFM converter to still face the risk of overheating damage after the grid fault is cleared.

It is worth noting that the large signal model in (4) is not limited to the assumption of constant U_f. When considering the effect of a reactive power control loop [1], the terminal voltage $\mathbf{U}_f$ is determined by output reactive power following the droop principle, the voltage dynamic can be written as

$$U_f(E_s,\delta) = \left[u(E_s,\delta) + \sqrt{u(E_s,\delta)^2 + 4c}\right] \Big/ 2 \tag{5}$$

where Q_e and Q_0 are the output reactive power and its reference. K_q is the Q-V droop coefficient and U_0 is the reference of terminal voltage. $u(E_s, \delta)$ and c are

$$u(E_s,\delta) = E_s\cos\delta - X_{se}/K_q, c = X_{se}(Q_0 + U_0/K_q). \tag{6}$$

The expression of the transient current with reactive power voltage droop control is written as

$$I_e(\delta) = \sqrt{E_s^2 + U_f^2(E_s,\delta) - 2U_f(E_s,\delta)E_s\cos\delta} \Big/ X_{se}. \tag{7}$$

The transient current behavior with reactive power control loop effect can also be discussed using the above method.

In the light of the above analysis, the angle δ_{cr} is the dividing point for whether the ROC phenomenon occurs, so it is defined as CRA. The concept of CRA can qualitatively explain the occurrence of ROC, but power–angle swing motion introduced by the inertia of the GFM converter makes the actual CRA no longer an intersection point of the current power angle curve shown in Fig. 2. The quantitative characterization and calculation are necessary to accurately identify the ROC state with inertia effect, and it will be performed in the next section.

III. Depiction of Recovery Overcurrent Boundary

This section will deduce the power angle relationship in critical ROC status for ROC boundary description. On this basis, the ROC region is characterized and the quantitative calculation method of CRA is proposed to readily identify ROC status.

A. Angle Relationship in Critical Recovery Overcurrent State

The power angle will increase monotonically in the fault stage and decrease immediately after fault clearance without inertia effect. In this case, the maximum fault current and the maximum recovery current are both at the FCP as shown in Fig. 2, and CRA is the intersection point of $I_{ef}(\delta)$ curve and $I_{ep}(\delta)$ curve. However, the velocity at FCP is not zero, and there will be a deceleration process of power angle at the beginning of the fault recovery stage due to the inertia effect. In this case, although the recovery current may be less than the fault current at the fault clear moment, the recovery current continues to rise during the recovery stage and may eventually exceed the fault current. Therefore, the existence of inertia will make the real CRA smaller than the intersection point δ_{cr}. The case with symmetrical fault is utilized to illustrate the inertia effect and the accuracy of the proposed model, as shown in Fig. 3, where the fault grid voltage is 0.2 p.u. and the post fault grid voltage is 0.8 p.u. The parameters in Fig. 3 are shown in Table I and the inertia time constant H is adjusted to 6 s to highlight the inertia impact.

To accurately identify the occurrence of the ROC phenomenon with inertia effect, the critical ROC state in which the maximum fault current equals the maximum recovery current

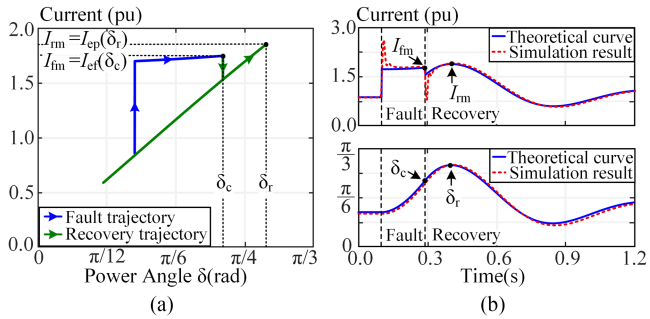

Fig. 3. Maximum current and its corresponding angle. (a) Current trajectory in the current power angle plane. (b) Current waveform in the time domain.

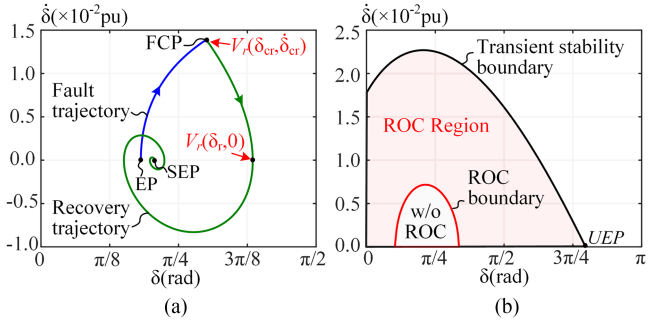

Fig. 4. ROC boundary characterization of GFM converter. (a) Power angle trajectory. (b) ROC boundary.

TABLE I
ELECTRICAL PARAMETERS OF EXPERIMENTAL PROTOTYPE

Category	Parameter	Value
System	Rated power S_N	6 kVA
	Rated frequency f_0	50 Hz
	Rated voltage (line-to-line) E_{sN}	190 V
	Equivalent system inductance L_{se}	9.8 mH (0.51 p.u.)
Converter hardware	Switching frequency f_{sw}	10 kHz
	Filter inductance L_f	860 μH (0.06 p.u.)
	Filter capacitance C_f	70 μF (0.1 p.u.)
GFM control	Terminal voltage reference U_{ref}	190 V (1 p.u.)
	Active power reference P_0	5 kW (0.83 p.u.)
	Damping coefficient D	35 p.u.
	Inertia time constant H	4 s

should be investigated first. For intuitive analysis, the fault voltage coefficient k_f and the recovery voltage coefficient k_r are defined because of the similarity in the description of the power angle relationship between the fault and recovery stage

$$k_f = E_f/E_s, k_r = E_r/E_s, P_{em} = U_f E_s/X_{se} \tag{8}$$

where $P_{\rm em}$ is the maximum transmission power of the grid-connected GFM converters under the rated grid voltage $E_{\rm s}$. To provide intuitive analysis and valid modeling accuracy, the time domain simulation results corresponding to the working conditions in Fig. 3(a) are given together with the solution results of the proposed model, as shown in Fig. 3(b).

In the fault stage, the power angle will continue to increase due to power deviation in (1). The first derivative of $I_{\rm e}(\delta)$ is

$$dI_e(\delta)/\delta = S_e(\delta)/(U_f|S_e(\delta)|) > 0 \forall \delta \in [0,\pi]. \tag{9}$$

Therefore, the current in the fault stage will increase with the angle monotonically and reach its maximum value at FCP, as the blue line in Fig. 3(a) indicates. The maximum fault current can be calculated with the clear angle $\delta_{\rm c}$ at FCP through (4) as follows:

$$I_{\rm fm} = I_{\rm ef}(\delta_c) = P_{\rm em}\sqrt{1+k_f^2-2k_f\cos\delta_c}\Big/X_{se}. \tag{10}$$

After the fault is cleared, the inertia of the GFM converter will force the angle to continuously increase until the velocity reaches zero at the angle $\delta_{\rm r}$, which causes the current to become larger in this process, as the green line in Fig. 3(a) shows. Thus, the current in the recovery stage will reach its maximum value $I_{\rm rm}$ at $\delta_{\rm r}$ due to the monotonicity of the current power angle curve shown in (9), as shown in Fig. 3(b). The expression of $I_{\rm rm}$ is shown as

$$I_{\rm rm} = I_{ep}(\delta_r) = P_{\rm em}\sqrt{1+k_r^2-2k_r\cos\delta_r}\Big/X_{se}. \tag{11}$$

Based on the expression of maximum fault current and recovery current, the power angle relationship between $\delta_{\rm c}$ and $\delta_{\rm r}$ in critical ROC state is obtained through $I_{\rm fm}=I_{\rm rm}$, and in this situation, the power angle $\delta_{\rm c}$ at FCP also satisfies the definition of CRA, i.e., $\delta_{\rm c}=\delta_{\rm cr}$. Thus, the angle condition is deduced from (10) and (11) as

$$\cos\delta_{cr} = (k_r/k_f)\cos\delta_r + \left(k_f^2-k_r^2\right)/2k_f. \tag{12}$$

This equation transforms the current constraint into the CRA-related condition, which can be used for ROC boundary depiction.

B. Recovery Overcurrent Region Characterization

It is worth noting that the power angle $\delta_{\rm cr}$ corresponding to the maximum fault current is also located at the fault clear moment and the velocity at maximum recovery position $\delta_{\rm r}$ exactly equals zero. The dual properties of these two angles make them also subject to the constraints of the angle swing motion, which can be intuitively characterized by the classical Lyapunov function in transient stability analysis [9], [15].

The power angle motion is illustrated in the phase plane, as shown in Fig. 4(a). The total transient energy during the fault recovery stage of the grid-connected GFM converter includes kinetic energy and potential energy, which can be written as

$$V_r\left(\delta,\dot{\delta}\right) = H\dot{\delta}^2\Big/2 - \delta P_0 - k_r P_{em}\cos\delta + E_0 \tag{13}$$

where E_0 is a constant to present the potential energy reference. Since the velocity at the power angle $\delta_{\rm r}$ equals zero, the kinetic energy of the converter at this position is also zero. Setting $\delta_{\rm r}$ as a zero potential energy position can greatly simplify the calculation of energy function. When the power angle $\delta_{\rm r}$ is assumed to be zero potential energy position, E_0 is

$$E_0 = P_0\delta_r + k_r P_{em}\cos\delta_r. \tag{14}$$

On substituting (14) into (13), the Lyapunov function in the recovery process can be written as

$$V_r\left(\delta,\dot{\delta}\right)=H\dot{\delta}^2\Big/2+P_0\left(\delta_r-\delta\right)+k_rP_{em}(\cos\delta_r-\cos\delta). \tag{15}$$

Since the kinetic energy at $\delta_{\rm r}$ equals zero, the sum of kinetic energy and potential energy at FCP is totally converted into the potential energy at $\delta_{\rm r}$. Obviously, the minus potential energy at $\delta_{\rm r}$ guarantees that neither the power angle nor the current will continue to increase, and thus the ROC boundary can be characterized in phase plane with condition (12) and energy relationship given by the following equation, which is shown in red line at Fig. 4(b):

$$V_r\left(\delta_{cr},\dot{\delta}_{cr}\right)=V_r\left(\delta_r,0\right)=0. \tag{16}$$

The transient stability boundary can be characterized by the Lyapunov function with UEP in post fault [11], where UEP is one of the equilibrium points of grid-connected GFM converter with $dP/d\delta<0$ in post fault condition, and it is calculated as

$$\delta_{eu}=\pi-\arcsin\left(\frac{P_0}{k_rP_{\rm em}}\right). \tag{17}$$

The ROC boundary divides the attraction domain of the GFM converter into two parts, as shown in Fig. 4(b). The red area is the ROC region and the converter will face ROC problems if FCP at this region. If the fault is cleared in the gray area, the ROC problem can be avoided. The ROC phenomenon would happen when the angle and velocity at FCP are large, as larger active power is needed to complete the angle deceleration in the recovery stage and larger reactive power is required to support the voltage, which results in the ROC region being outside.

The region without ROC means that the OCC of the GFM converter is mainly used in fault grid support. It is more suitable for a converter with limited and costly OCC to operate in this area because the GFM converter does not need additional OCC for resynchronization and post-fault grid support. Based on the above analysis, the ROC boundary could be changed to be as close to the stability boundary as possible through the control structure improvement so that the GFM converter can utilize its limited and costly OCC in fault grid support. Moreover, it is more appropriate to output less active current to suppress the power angle acceleration and increase reactive current for fault grid support in the fault stage. In the recovery stage, the adjustment of active current is more important to achieve power angle deceleration and return to normal operation. This may provide some insight into GFM control optimization.

C. Critical Recovery Angle Calculation

The classical Lyapunov function can also characterize the transient energy during fault and it further can be used in the quantitative assessment of CRA with the energy function in the recovery stage. In this manner, whether the GFM converter enters the ROC region can be easily and effectively identified by comparing the fault clear angle $\delta_{\rm c}$ at FCP and CRA. The total energy during fault is equal to the total energy in the recovery process at FCP because the transient energy does not mutate. Thus, the total energy in the fault stage is written as

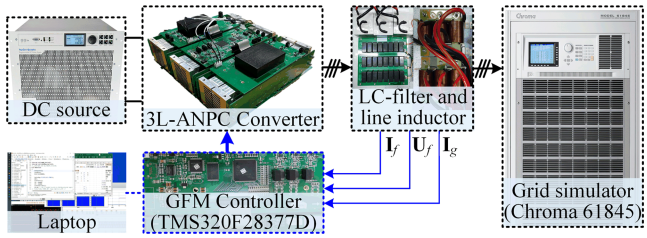

Fig. 5. Experimental setup of grid-connected GFM converter.

$$V_f\left(\delta,\dot{\delta}\right)=H\left(\dot{\delta}^2-\dot{\delta}_c^2\right)\Big/2-P_0\left(\delta-\delta_c\right)-k_fP_{em}(\cos\delta-\cos\delta_c)+V_r\left(\delta_c,\dot{\delta}_c\right). \tag{18}$$

Considering both fault and recovery characteristics, the transient energy constraint of CRA can be expressed as

$$\begin{cases}V_f\left(\delta_0,0\right)-V_f\left(\delta_{cr},\dot{\delta}_{cr}\right)=0\\ V_r\left(\delta_{cr},\dot{\delta}_{cr}\right)=0\end{cases} \tag{19}$$

and its expanded form is

$$\begin{cases}P_0\left(\delta_{cr}-\delta_0\right)+k_fP_{em}(\cos\delta_{cr}-\cos\delta_0)-H\dot{\delta}_{cr}^2\Big/2=0\\ P_0\left(\delta_r-\delta_{cr}\right)+k_rP_{em}(\cos\delta_r-\cos\delta_{cr})+H\dot{\delta}_{cr}^2\Big/2=0\end{cases}. \tag{20}$$

The relationship of total transient energy from SEP δ_0 to CRA δ_{cr} can be obtained by (20), which considers the dynamics of both fault and recovery stages. Meanwhile, the CRA is also the angle at FCP in a critical ROC state, and it satisfies the condition of (12). Therefore, energy constraints and current constraints can be combined for CRA calculation as

$$\begin{cases}0=P_0(\delta_0-\delta_r)+k_fP_{em}\cos\delta_0+P_{em}(k_f^2-k_r^2)/2\\ -(2k_f-k_r)P_{em}\cos\delta_{cr}\\ \delta_r=\arccos\left[(k_f/k_r)\cos\delta_{cr}-\left(k_f^2-k_r^2\right)\Big/2k_r\right]\end{cases}. \tag{21}$$

By solving (21), CRA can be directly and quantitatively calculated for ROC state identification with inertial effect. In particular, when the GFM converter has no inertia, the CRA can be simplified to

$$\delta_{cr}=\arccos\left[\left(k_f^2-k_r^2\right)/2\left(k_f-k_r\right)\right]. \tag{22}$$

Its physical meaning is the intersection point of $I_{\rm ef}(\delta)$ curve and $I_{\rm ep}(\delta)$ curve as shown in Fig. 2. Therefore, the proposed method can be applied to both the transient current analyses of the GFM converter with and without inertia effect.

IV. Experiment Verification

The correctness and effectiveness of ROC boundary characterization and CRA calculation are tested in a 6-kVA GFM converter platform with 10 kHz switching frequency shown in Fig. 5, with parameters in Table I. In the GFM converter, the damping coefficient D is equivalent to the reciprocal of the

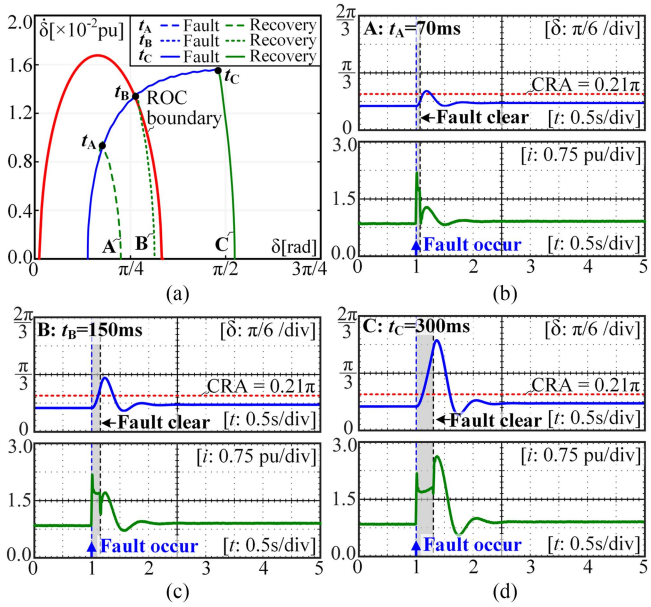

Fig. 6. Comparison of theoretical ROC boundary and experimental results with $H = 4$ s and $X_{se} = 0.51$ p.u. using different FCTs. (a) Phase portrait. (b) $t_A = 70$ ms. (c) $t_B = 150$ ms. (d) $t_C = 300$ ms.

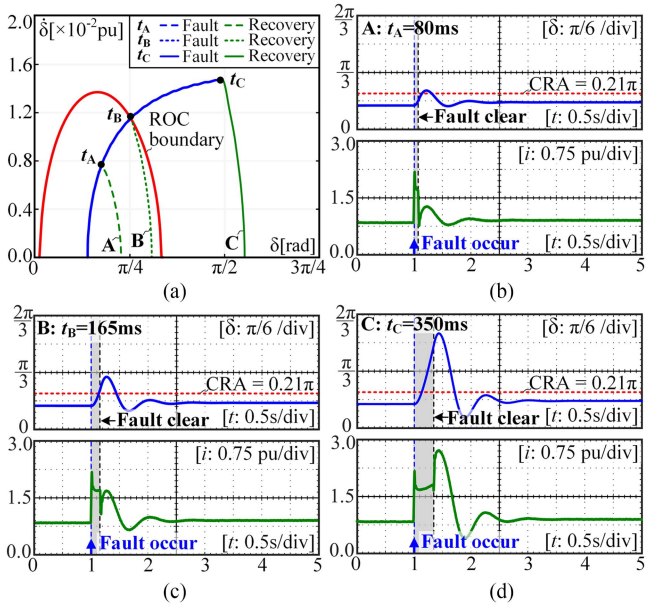

Fig. 7. Comparison of theoretical ROC boundary and experimental results with $H = 6$ s and $X_{se} = 0.51$ p.u. using different FCTs. (a) Phase portrait. (b) $t_A = 80$ ms. (c) $t_B = 165$ ms. (d) $t_C = 350$ ms.

active power–frequency droop coefficient, which is generally determined by grid code, and its typical value is set around 20–35 p.u. Therefore, D is chosen as 35 p.u. [18], [19]. Since the power angle motion and the output current trajectory of the GFM converter are dominated by its control loop, and are not affected by the topology, this letter chooses the three-level ANPC as the converter topology in the experiment.

An experimental test with $D = 35$ p.u., $H = 4$ s, $U_{ref} = 1$ p.u., $X_{se} = 0.51$ p.u., and $P_0 = 0.83$ p.u. is studied and shown in Fig. 6. The grid voltage symmetrically drops to 0.1 p.u. at 1 s and recovers to 0.9 p.u. with different fault clear time (FCT) configured by grid simulator. The theoretical ROC boundary is characterized using the method in Section III-B and shown in Fig. 6(a) as the red line, the fault and recovery trajectories of the GFM converter with FCT $t_A = 70$ ms, $t_B = 150$ ms, and $t_C = 300$ ms are also illustrated in Fig. 6(a). The corresponding experimental results are shown in Fig. 6(b)–(d), and the theoretical CRA calculated with (14) is also illustrated by a red dashed line in Fig. 6(b)–(d). In case A, the fault is cleared in the region without ROC and the clear angle δ_c at FCP is lower than CRA, so the on-fault current of the GFM converter is larger than the current in the recovery stage in Fig. 6(b). It is worth noting that FCP is close to the ROC boundary and the clear angle is also approximately equal to CRA in case B, the fault current and recovery current are nearly the same in Fig. 6(c). If the fault is cleared in the ROC region, as shown in Fig. 6(d), the ROC phenomenon occurs because δ_c is larger than CRA. The results are very consistent with theoretical analysis.

Another test with a larger inertia constant $H = 6$ s is also studied, and the other settings are the same as above. The ROC boundary is shown in Fig. 7(a) and the experimental results are presented in Fig. 7(b)–(d). The ROC does not occur because the fault is cleared before CRA in Fig. 7(b). The recovery current rises to the fault current if the FCP is near the ROC boundary in Fig. 7(c). The ROC occurs in Fig. 7(d), where δ_c is larger than CRA. It matches the theoretical analysis well.

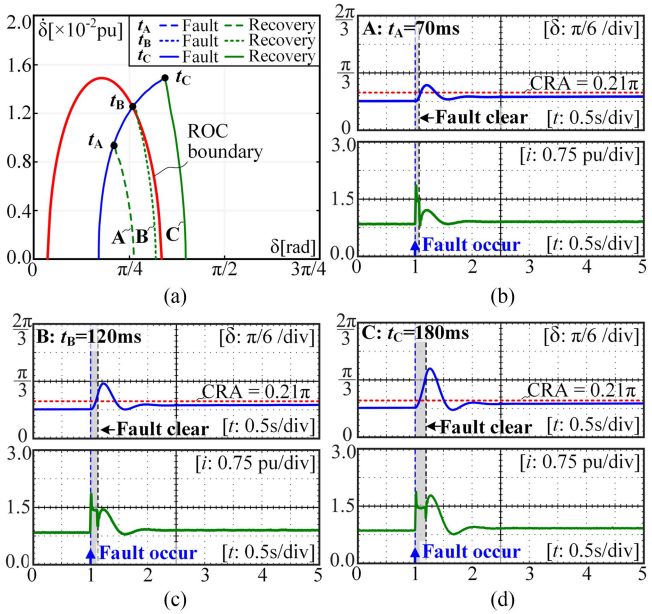

Fig. 8. Comparison of theoretical ROC boundary and experimental results with $H = 4$ s and $X_{se} = 0.6$ p.u. using different FCTs. (a) Phase portrait. (b) $t_A = 70$ ms. (c) $t_B = 120$ ms. (d) $t_C = 180$ ms.

To validate the effectiveness of the proposed method under different grid impedance conditions, the experimental test with a larger equivalent impedance $X_{se} = 0.6$ p.u. is studied, and the other settings are the same as the case with $H = 4$ s. The ROC boundary is illustrated in Fig. 8(a) and the experimental results are presented in Fig. 8(b)–(d). In the critical ROC state

in Fig. 8(c), the magnitude of fault current and recovery current is equal. When the FCP is smaller than CRA in Fig. 8(b), the fault current is larger, otherwise, the recovery current is larger, as shown in Fig. 8(d). The result matches the theoretical analysis very well.

The above experimental results validate the effectiveness of the proposed ROC boundary and CRA calculation method.

V. Conclusion

This letter describes the current trajectories of a GFM converter in the current power angle plane to reveal the ROC mechanism with the CRA concept. On top of that, the power angle relationship in the critical ROC state is deduced from the transient current constraint, and the ROC region is further characterized quantitatively. Moreover, an analytical method for CRA calculation is proposed to readily identify whether the ROC state occurs. Experimental results validate the effectiveness of the proposed method. This letter reveals the inherent relationship between current behavior and power angle swing motion of GFM control during grid fault transients, and it may provide some new insights for transient analysis and control optimization of the GFM converter.

References

[1] R. Rosso, X. Wang, M. Liserre, X. Lu, and S. Engelken, "Grid-forming converters: Control approaches, grid-synchronization, and future trends—A review," *IEEE Open J. Ind. Appl.*, vol. 2, pp. 93–109, 2021.

[2] H. Wu and X. Wang, "Control of grid-forming VSCs: A perspective of adaptive fast/slow internal voltage source," *IEEE Trans. Power Electron.*, vol. 38, no. 8, pp. 10151–10169, Aug. 2023.

[3] L. Huang, H. Xin, Z. Wang, L. Zhang, K. Wu, and J. Hu, "Transient stability analysis and control design of droop-controlled voltage source converters considering current limitation," *IEEE Trans. Smart Grid*, vol. 10, no. 1, pp. 578–591, Jan. 2019.

[4] T. Qoria, F. Gruson, F. Colas, G. Denis, T. Prevost, and X. Guillaud, "Critical clearing time determination and enhancement of grid-forming converters embedding virtual impedance as current limitation algorithm," *IEEE J. Emerg. Sel. Topics Power Electron.*, vol. 8, no. 2, pp. 1050–1061, Jun. 2020.

[5] B. Fan, T. Liu, F. Zhao, H. Wu, and X. Wang, "A review of current-limiting control of grid-forming inverters under symmetrical disturbances," *IEEE Open J. Power Electron.*, vol. 3, pp. 955–969, 2022.

[6] W. Shao et al., "A power module for grid inverter with in-built short-circuit fault current capability," *IEEE Trans. Power Electron.*, vol. 35, no. 10, pp. 10567–10579, Oct. 2020.

[7] S. Bhadoria et al., "Enablers for overcurrent capability of silicon-carbide-based power converters: An overview," *IEEE Trans. Power Electron.*, vol. 38, no. 3, pp. 3569–3589, Mar. 2023.

[8] F. Mandrile, F. Stella, E. Carpaneto, and R. Bojoi, "Grid fault current injection using virtual synchronous machines featuring active junction temperature limitation of power devices," *IEEE Trans. Emerg. Sel. Topics Power Electron.*, vol. 10, no. 5, pp. 6243–6251, Oct. 2022.

[9] J. Lei, X. Xiang, B. Liu, W. Li, and X. He, "Quantitative and intuitive VSG transient analysis with the concept of damping area approximation," *IEEE Trans. Smart Grid*, vol. 14, no. 3, pp. 2477–2480, May 2023.

[10] X. Fu et al., "Large-signal stability of grid-forming and grid-following controls in voltage source converter: A comparative study," *IEEE Trans. Power Electron.*, vol. 36, no. 7, pp. 7832–7840, Jul. 2021.

[11] Z. Shuai, C. Shen, X. Liu, Z. Li, and Z. J. Shen, "Transient angle stability of virtual synchronous generators using Lyapunov's direct method," *IEEE Trans. Smart Grid*, vol. 10, no. 4, pp. 4648–4661, Jul. 2019.

[12] D. Pan, X. Wang, F. Liu, and R. Shi, "Transient stability of voltage-source converters with grid-forming control: A design-oriented study," *IEEE Trans. Emerg. Sel. Topics Power Electron.*, vol. 8, no. 2, pp. 1019–1033, Jun. 2020.

[13] F. Zhao, Z. Shuai, W. Huang, Y. Shen, Z. J. Shen, and C. Shen, "A unified model of voltage-controlled inverter for transient angle stability analysis," *IEEE Trans. Power Del.*, vol. 37, no. 3, pp. 2275–2288, Jun. 2022.

[14] M. H. Ravanji, W. Zhou, N. Mohammed, and B. Bahrani, "Comparative analysis of the power output capabilities of grid-following and grid-forming inverters considering static, dynamic, and thermal limitations," *IEEE Trans. Power Syst.*, vol. 39, no. 2, pp. 2693–2705, Mar. 2024.

[15] M. Li et al., "Analysis and improvement of large-disturbance stability for grid-connected VSG based on output impedance optimization," *IEEE Trans. Power Electron.*, vol. 37, no. 8, pp. 9807–9826, Aug. 2022.

[16] K. Sun, W. Yao, J. Wen, and L. Jiang, "A two-stage simultaneous control scheme for the transient angle stability of VSG considering current limitation and voltage support," *IEEE Trans. Power Syst.*, vol. 37, no. 3, pp. 2137–2150, May 2022.

[17] H. Wu and X. Wang, "Design-oriented transient stability analysis of grid-connected converters with power synchronization control," *IEEE Trans. Ind. Electron.*, vol. 66, no. 8, pp. 6473–6482, Aug. 2019.

[18] *IEEE Standard for Interconnection and Interoperability of Distributed Energy Resources with Associated Electric Power Systems Interfaces*, IEEE Std. 1547-2018, 2018.

[19] *Requirements for Micro-Generating Plants to be Connected in Parallel with Public Low-Voltage Distribution Networks*, BS EN 50438:2013, 2013.